Faraday Discussions

Accepted Manuscript

This manuscript will be presented and discussed at a forthcoming Faraday Discussion meeting. All delegates can contribute to the discussion which will be included in the final volume.

Register now to attend! Full details of all upcoming meetings: http://rsc.li/fd-upcoming-meetings

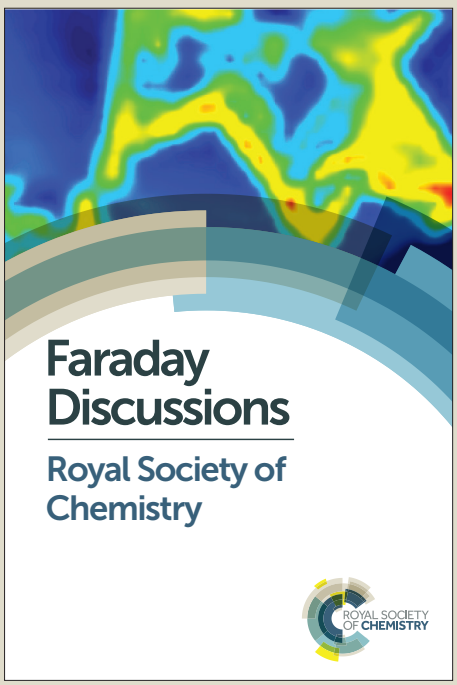

This is an *Accepted Manuscript*, which has been through the Royal Society of Chemistry peer review process and has been accepted for publication.

Accepted Manuscripts are published online shortly after acceptance, before technical editing, formatting and proof reading. Using this free service, authors can make their results available to the community, in citable form, before we publish the edited article. We will replace this *Accepted Manuscript* with the edited and formatted *Advance Article* as soon as it is available.

You can find more information about *Accepted Manuscripts* in the Information for Authors.

Please note that technical editing may introduce minor changes to the text and/or graphics, which may alter content. The journal's standard Terms & Conditions and the Ethical guidelines still apply. In no event shall the Royal Society of Chemistry be held responsible for any errors or omissions in this *Accepted Manuscript* or any consequences arising from the use of any information it contains.

ROYAL SOCIETY OF CHEMISTRY

www.rsc.org/faraday_d

A low cost synthesis method for functionalised iron oxide nanoparticles for magnetic hyperthermia from readily available materials

Joseph C. Bear,*[a] Bin Yu,[a,] Cristina Blanco-Andujar,[b] Paul D. McNaughter,[c] Paul Southern,[b] Marc-Krystelle Mafina,[d] Quentin A. Pankhurst[b] and Ivan P. Parkin[a]

Received (in XXX, XXX) Xth XXXXXXXXX 200X, Accepted Xth XXXXXXXXX 200X
First published on the web Xth XXXXXXXXX 200X
DOI: 10.1039/b00000000x

The synthesis of iron oxide nanocrystals from reagents taken from high street sources using thermal decomposition of an iron-fatty acid precursor in a high boiling point solvent in the presence of surfactants is presented. The nanocrystals were characterised using a variety of techniques including: electron microscopy, X-ray dispersive spectroscopy, infrared spectroscopy, X-ray diffraction, X-ray photoelectron spectroscopy and magnetometry. Thermogravimetric analysis is also used to compare the decomposition behaviour of iron oleate and iron palmitate, our nanoparticle precursors. The nanoparticles also exhibit shape anisotropy when prepared under optimum conditions. We show that these nanoparticles have potential in magnetic hyperthermia after transfer to aqueous media *via* an amphiphilic polymer.

Introduction

The large scale and inexpensive synthesis of monodisperse nanocrystals from non-hazardous precursors is an area of intense interest in nanoparticulate research.[1–5]

Synthesis methods such as continuous hydrothermal flow synthesis and ball milling generate kilogram-scale volumes of nanoparticles, but often at the expense of product crystallinity and monodispersity.[6–9] On the other hand, the nanoparticle quality control gained using hot-injection and "heat-up" methods is excellent.[3,10,11] However, these methods often utilise expensive reagents and are not applicable for large scale processes due to large temperature gradients placed across synthesis solutions. The vast majority of "heat-up" methods involve the thermal decomposition of iron-fatty acid complexes such as iron oleate. Iron-fatty acid complexes are either isolated and decomposed in the presence of surfactants[12] or formed *in situ*.[13] In their landmark paper, Hyeon and co-workers decomposed a pre-synthesised iron oleate complex in the presence of oleic acid and 1-octadecene to produce highly monodisperse and size-controllable Fe_3O_4 nanocrystals on a batch-level scale.[3] In their paper, they allude to the possibility of a scale-up process and draw attention to the inexpensive nature and low toxicity of the precursors (Figure 4, ESI).

In particular, iron oxide has received a great deal of interest for magnetic fluid hyperthermia (MFH); a cancer treatment which uses radiofrequency to heat up superparamagnetic magnetic nanoparticles *in vivo* to thermally ablate/treat tumour cells.[14–17] The best nanoparticles for MFH are often a compromise between size, biocompatibility, cost, ease of synthesis, ability to respond to an external stimulus and heating ability.[17–19] Iron oxide has been of particular interest due to its fulfilment of the majority of these desired properties.[20,21]

In this paper, we have developed a synthesis using a similar thermal decomposition method to the one developed by Hyeon *et al*., but with precursors solely bought from high street shops and supermarkets. We report the batch-synthesis of high-quality iron oxide nanocrystals at a fraction of the cost compared to the Hyeon paper. We also demonstrate their suitability and effectiveness for magnetic hyperthermia, after transfer to aqueous media via amphiphilic polymer coating.[22,23]

The nanoparticles demonstrate significant temperature rises at low nanoparticle concentrations, particularly the nanostructures obtained from the decomposition of iron palmitate in shark liver oil. Therefore, the methods and reagents proposed in this paper represent a viable, facile and cheap route to effective hyperthermia agents.

Experimental details

Characterisation techniques

Transmission electron microscopy (TEM) images were recorded using a JEOL JEM 1200EX with a 4 megapixel Gatan Orius SC200 charge-coupled device (CCD) camera at an acceleration voltage of 120 kV. High resolution transmission electron microscopy (HRTEM) measurements were collected using a Philips CM200 FEG TEM fitted with a Gatan GIF 200 imaging filter and an Oxford Instruments UTW EDX detector running ISIS software. X-ray photoelectron spectroscopy (XPS) measurements were recorded on a Thermo Scientific K-alpha spectrometer. X-ray diffraction patterns were obtained on a PanAlytical diffractometer using Co Kα radiation, λ = 1.789010 Å. ATR-FTIR measurements were taken over a range of 450 to 4000 cm^{-1} using a Perkin-Elmer Spectrum-100 equipped with a universal ATR attachment. Magnetisation data was taken using a Quantum Design MPMS SQUID VSM Magnetometer (San Diego, USA) at 300 K using a field range of ±7 T. Mössbauer spectroscopy was carried out using a SEE Co. Model W302 Resonant Gamma Ray Spectrometer, with a ^{57}Co(Rh) gamma ray source operating at 300K. Isomer shifts were measured relative to α-Fe at 300K. Hyperthermia experiments were carried out using a

Faraday Discussions Accepted Manuscript

MACH system (Magnetic Alternating Current Hyperthermia) designed and built by Resonant Circuits Limited.[24] The temperature was monitored using a fluoroptic temperature probe (Luxtron FOT Lab Kit, Lumasense California USA).

Materials

Iron(III) chloride hexahydrate (98 %) was purchased from VWR International Ltd. Iron tablets were purchased from Boots Ltd. Olive oil and "Sainsbury basics" soap was purchased form J. Sainsbury Ltd. Shark liver oil (60 x 1000 mg capsules) was purchased from Shark Liver Oil UK.

All other laboratory chemicals used in this investigation were purchased from Sigma-Aldrich Chemical Co; including: 1-octadecene (technical grade, 90 %), oleic acid (technical grade, 90%), oleylamine (technical grade, ≤70%), poly(maleic anhydride-*alt*-1-octadecene) (average M_n = 30,000 – 50,000), tetramethyl ammonium hydroxide pentahydrate (≥97%) and sodium oleate (≤82% fatty acid content). Laboratory solvents were purchased from Fisher Scientific Ltd. and of the highest possible grade.

Nanoparticle synthesis and functionalisation.

Iron oxide nanoparticle synthesis. Iron oxide nanoparticles were synthesised by thermal decomposition of iron oleate, according to Park *et al.*[3] The iron oleate was prepared by heating a suspension of iron(III) chloride hexahydrate (10.8 g, 40 mmol) and sodium oleate (36.5 g, 120 mmol) in a solvent mixture of *n*-hexane (140 ml), deionised water (60 ml) and ethanol (80 ml) to 70 ºC for 4 hours. The organic layer was separated and washed with washed with 3 × 30ml portions of distilled water to remove sodium chloride. The dark brown organic layer was separated and dried *in vacuo*, to remove hexane, and isolated as a waxy solid (yield ~70 %).

Iron oleate (18.0 g, 20 mmol) and oleic acid (2.35 ml, 10 mmol) were dissolved in 1-octadecene (100 g, 396.1 mmol) and stirred thoroughly at room temperature. The reaction mixture was heated to 320 ºC at a rate of 3.3 ºC/min under nitrogen and held at 320 ºC for 1 hour. The resulting black solution was allowed to cool to room temperature before addition of ethanol (250 ml) to precipitate the particles. The solution was centrifuged at 600 *g* for 10 minutes, giving solid particle precipitates. If the precipitate was not solid, excess oleate-type species were removed by washing with ethanol (2 x 80 ml). The supernatant was discarded and the solid particle precipitates dispersed in chloroform (30 ml total).

Modified Fe_3O_4 nanoparticle synthesis. Iron palmitate was prepared by heating a suspension of homogenised iron tablets (20 tablets each containing 14 mg of iron as iron gluconate) and soap (assumed to be 65% sodium palmitate, 0.321 g, 1.15 mmol) in a solvent mixture of *n*-hexane (140 ml), deionised water (60 ml) and ethanol (80 ml) to 70 ºC for 4 hours. The organic layer was separated and washed with 3 × 30 ml portions of distilled water to remove sodium chloride. The dark organic layer was dried *in vacuo* to remove hexane, yielding the iron oleate complex as a waxy solid.

For ~12 nm particles and rods. Iron palmitate (2 g, 2.4 mmol) and olive oil (65 % oleic acid, 0.59 ml, 1.2 mmol) were dissolved in 1-octadecene (20 ml, 62.5 mmol) or shark liver oil (20 ml) and stirred thoroughly at room temperature. A molar ratio of 1:1 iron palmitate to the oleic acid content of olive oil to grow the rods (figure 2, (E) and (F)), whilst the solvent was changed to shark liver oil. The reaction mixture was heated to 320 ºC at a rate of 3.3 ºC/min under nitrogen and held at 320 ºC for 1 hour. The resulting black solution was allowed to cool to room temperature before addition of ethanol (250 ml) to precipitate the particles. The solution was centrifuged at 600 *g* for 10 minutes, giving solid particle precipitates. If the precipitate was not solid, excess fatty acid-type species were removed by washing with ethanol (2 x 80 ml). The supernatant was discarded and the solid particle precipitates dispersed in chloroform (30 ml total).

Phase transfer of iron oxide nanoparticles.

Oleic acid coated nanoparticles were transferred from organic solvents to water according to a protocol developed by Lees *et al.*[22] Iron oxide nanoparticles in hexane (5 ml) were precipitated with ethanol (~100 ml), centrifuged and the solid residue re-dispersed in chloroform (10 ml). Poly(maleic anhydride-*alt*-1-octadecene) (10 mg) was dissolved in chloroform (10 ml) and added under vigorous stirring to the nanoparticle solution and left to stir for 1 hour. The chloroform was removed slowly *in vacuo* (750 mbar, 25 °C water bath) and then subsequently placed under a ~10^{-2} mbar vacuum for 24 hours. 20 ml of a 0.1 M solution of tetramethyl ammonium hydroxide was added, and left overnight to react. Once the nanoparticles were fully dispersed, the solution was acidified to pH 8 with acetic acid before concentration with centrifuge filters (Centriprep YM-10, 10 kDa MW cutoff for 3 × 20 minute cycles at 3000 *g*).

Magnetic hyperthermia testing.

A sample of polymer coated water-transferred iron oxide nanoparticles 1ml was placed into a 1.5ml Eppendorf® tube and situated centrally in a 6 turn room temperature controlled solenoid coil within the MACH system. An alternating field strength of 6.6 kA/m at a frequency of 945 kHz was used throughout the magnetic hyperthermia experiments. The experiment was run until the sample reached temperature saturation, typically in the order of five minutes. Temperature data was collected using a non-metallic fluoroptic probe in order to prevent eddy current heating within the sample.

Results and discussion.

Colloidal iron oxide nanoparticles were prepared using the high temperature thermal decomposition of iron-fatty acid complexes in the presence of surfactants. Reaction solutions turned from brown to black during the reaction, indicating the formation of colloidal nanoparticles. Nanoparticles were isolated by precipitation with ethanol and centrifugation and

Faraday Discussions Accepted Manuscript

dispersed readily in hexane. It is noteworthy that obtained samples had significant organic components which were difficult to remove without the use of magnetic separation.

Three different samples of iron oxide nanoparticles were prepared herein, as illustrated in scheme 1. Sample **(I)** are nanoparticles prepared from laboratory reagents according to the procedure reported by Park.[3] Sample **(II)** and **(III)** are both prepared from high street reagents, only differing in the solvent used for the decomposition step.

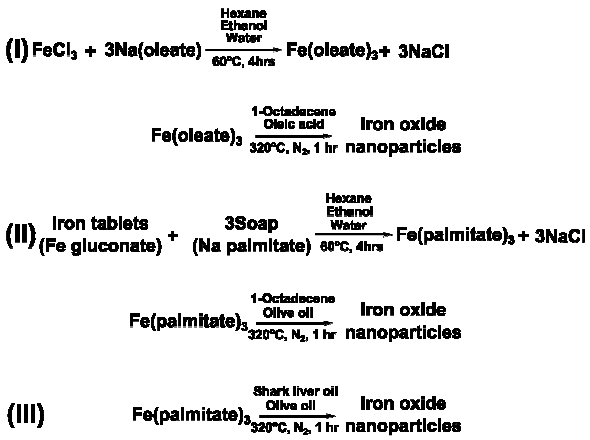

[Scheme 1: Sample **(I)** is the route to iron oxide nanoparticles proposed by Park *et al.*[3], Sample **(II)** is the synthesis of iron palmitate from high street sources and its subsequent decomposition in 1-octadecene and Sample **(III)** the decomposition of iron palmitate in shark liver oil.]

The obtained nanoparticles from all reactions were highly crystalline and colloidally stable in organic solvents due to the blanket surface coverage of palmitic acid. This was confirmed by ATR-FTIR analysis as carbonyl stretches are clearly observable on the nanoparticle surfaces at *ca.* 1700 cm^{-1}. Weak stretches from iron oxide (Fe-O) bonds are observed in the fingerprint region (*ca.* 500 cm^{-1}).

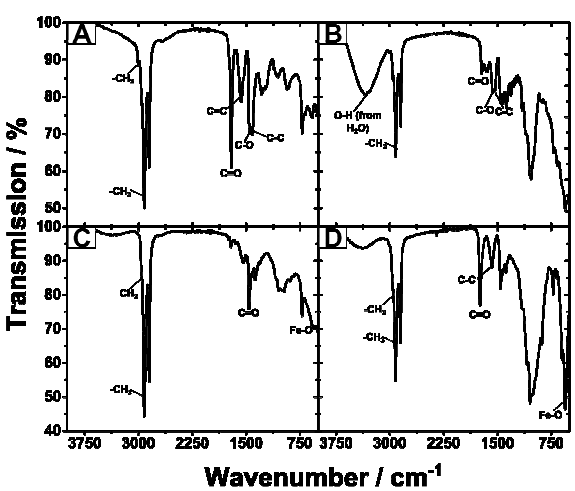

[Figure 1: ATR-FTIR spectra of: iron-oleate (A), iron oxide nanoparticles obtained from the decomposition of iron-oleate, (Sample (**I**)) (B), iron-palmitate from iron tablets (C) and nanoparticles obtained from iron-palmitate decomposition in shark liver oil (Sample (**III**) (D).]

TEM analysis showed a high degree of monodispersity in all samples of iron oxide nanoparticles. The shape of the NPs was predominantly spherical using iron-oleate or iron palmitate as the iron precursor (figure 2). It was found that the solvent affected the final shape of the products. When a high ratio of oleic acid to iron palmitate was used for the decomposition in shark liver oil, epitaxial growth of nanorods, as well as iron oxide nanoparticles, was observed (figure 2E).

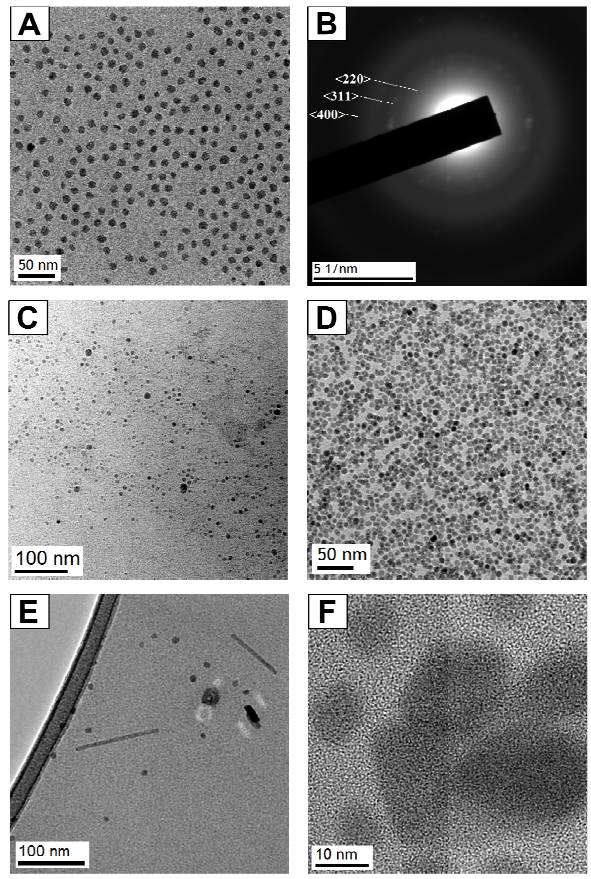

[Figure 2: Iron oxide nanoparticles from the decomposition of iron palmitate in 1-octadecene (Sample (**II**)) (A). SAED of iron oxide nanoparticles from the decomposition of iron palmitate in 1-octadecene (B). Iron oxide nanoparticles from the decomposition of iron palmitate in shark liver oil (Sample (**III**)) (C). Iron oxide nanoparticles synthesised according to *Park et al.*[3] (Sample (**I**))(D). Iron oxide obtained from a 1:1 molar ratio of olive oil (oleic acid) to iron palmitate in shark liver oil. HRTEM micrograph of a single iron oxide nanoparticle from a 1:1 ratio of iron palmitate shark liver oil (F).]

These nanorods were highly crystalline, readily dispersible in organic solvents and exhibited epitaxial growth. The nanorods however, were not composed of iron oxide, moreover of rhenanite (β-$NaCaPO_4$), determined by EDX and XRD. Ingredients from the initial iron tablets such as calcium phosphate and sodium chloride contributed to the nanorod formation. This is possibly due to the organic species present in shark liver oil.

The constituents of shark liver oil itself vary according to

Faraday Discussions Accepted Manuscript

the depths the shark normally resides.[25–28] Deep-sea sharks can approach neutral buoyancy through storage of low density lipids stored in the liver. A large contributor is squalene (density 0.858 g/ml at 25°C, and increases at cold, deep sea temperatures) which has been shown to influence iron oxide nanoparticle shape.[29] Other constituents include: diacyl glyceryl ether, triacylgycerol and wax esters, all of which could contribute to directional growth of nanoparticles.[30–33]

By varying the amount of oleic acid used in the synthesis, the particle size could be tuned, with particle size increasing with smaller amounts of oleic acid (*viz* olive oil). Average NP sizes were calculated from TEM micrographs, which were calculated to be ~12.7, 5.8 and 3.6 nm for 1.2, 6, 24 mmol of oleic acid in olive oil respectively (when decomposing 2 g of iron palmitate).

EDX analysis detailed the elemental composition of the nanoparticles, confirming the presence of iron and oxygen. EDX and XPS analyses also highlighted additional elementals acquired from the initial iron tablets such as phosphorus and calcium (*vide infra*).

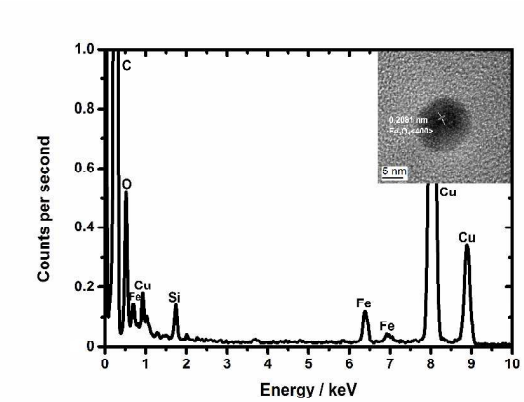

[Figure 3: (Main) EDX spectrum of iron oxide nanoparticles from iron palmitate decomposed in shark liver oil (Sample **(III)**) and (inset) HRTEM micrograph of a spherical iron oxide nanoparticle, showing the <400> plane of Fe_3O_4.]

The decomposition of iron palmitate and iron oleate species was followed by thermo-gravimetric analysis (TGA). Both iron oleate and iron palmitate samples had very similar decomposition profiles. The primary decomposition temperatures varied slightly between the two samples, but resided between 190 and 210 ºC, after which rapid decomposition occurred. There was a significant loss of mass in the iron palmitate sample between 30 and 80 ºC, which is associated with the evaporation of residual ethanol from the washing process.

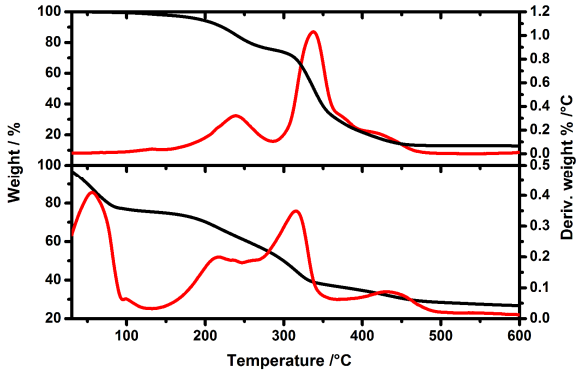

[Figure 4: TGA traces with first derivatives of iron oleate (above) and iron-palmitate (below)]

Particle composition and structure was analysed by X-ray photoelectron spectroscopy (XPS) and X-ray diffraction (XRD). XRD analysis yielded a pattern consistent with that of an inverse spinel structure γ-Fe_2O_3/Fe_3O_4; however, it was not possible to discern between the two structures due to the high degree of similarity between the profiles of these two structures. The nanostructures obtained from a 1:1 molar ratio of olive oil to iron palmitate indicated the presence of a multiphase system as seen from XRD analysis (figure 6 ESI). The sample was found to be mainly constituted by two phases due to the presence of peaks consistent with the diffraction pattern of γ-Fe_2O_3/Fe_3O_4 and also peaks corresponding to the orthorhombic structure of rhenanite.

XPS analyses revealed that the surface composition of the nanoparticles was influenced heavily by ingredientss in the precursor, namely dicalcium phosphate (E341) which is used as a tableting agent. Calcium has been shown to be an effective dopant for iron oxide,[34,35] and iron oxide surfaces have high affinity for phosphorus containing ligands,[36] hence the high level of surface doping. EDX analysis showed that Ca and P were indeed dopants for the iron, albeit constituting *ca*. 4% of the total nanoparticle mass.

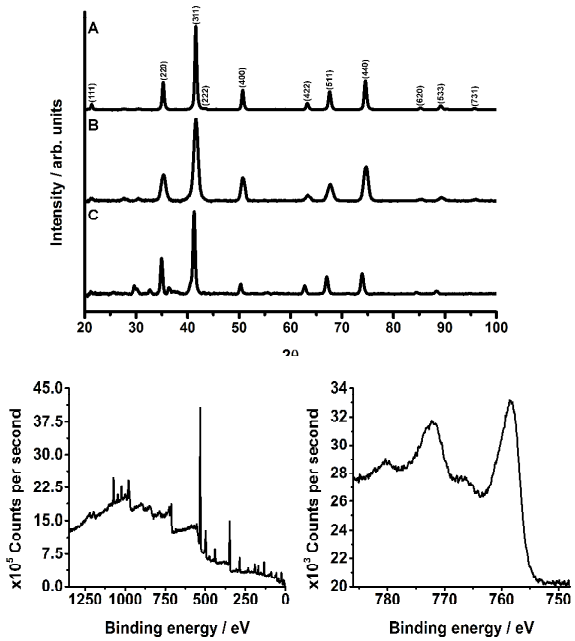

[Figure 5: (Top) XRD patterns of A) Magnetite standard, B) iron oxide nanoparticles from standard reagents (Sample **(I)**)

Faraday Discussions Accepted Manuscript

C) Sample **(II)** (Bottom) Survey and Fe2p XPS spectra of iron oxide from iron palmitate decomposed in shark liver oil (Sample **(III))**]

Mössbauer spectroscopy offers insights into the oxidation states and chemical environments of iron atoms present in the iron oxide lattice. All spectra were taken at room temperature. Analysis of the nanoparticles synthesised according to Park gave a very broad single peak, with wings extending out to ± 10 mm/s. The latter indicates the presence of magnetic hyperfine absorption, as would be expected in a magnetic iron oxide (such as maghemite or magnetite) below its superparamagnetic blocking temperature. The very broad nature of the absorption could be due to temporal or structural factors, or both – i.e. temporal as in magnetic relaxation on the nanosecond timescale of the Mössbauer measurement, or structural as in the crystallinity, size or defect structure of the particles. Further experiments would be needed to clarify this.

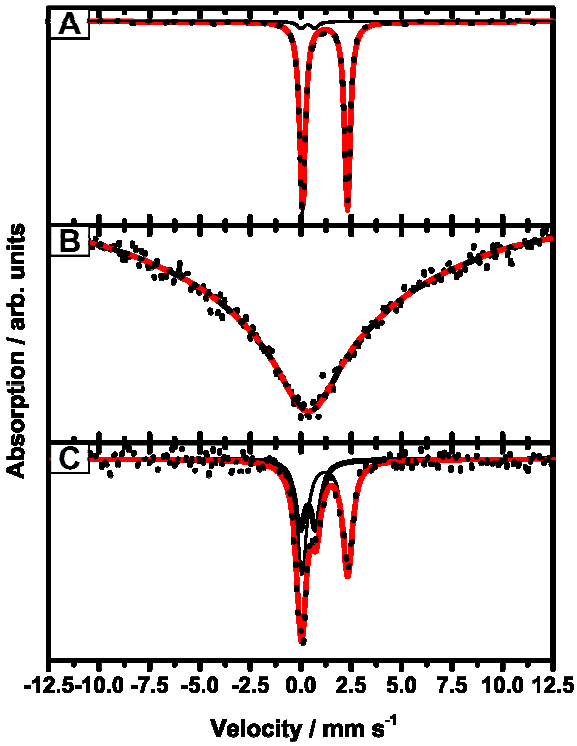

[Figure 6: ^{57}Fe Mössbauer spectra of: homogenised iron tablets (A), iron oxide nanoparticles from standard reagents (Sample **(I))** (B), iron oxide nanoparticles from the decomposition of iron palmitate in shark liver oil (Sample **(III))** (C). The red trace represents the fit with the thick black line the Fe^{3+} doublet component and the thin black line the Fe^{2+} doublet component.]

Mössbauer analysis of Sample **(III)** shows the superposition of two doublets – one of which has parameters typical of Fe^{3+} (isomer shift δ = 0.30 ± 0.07 mm/s and quadrupole splitting Δ = 0.70 ± 0.17 mm/s), and another with parameters typical of Fe^{2+} (δ = 1.18 ± 0.04 mm/s and Δ = 2.27 ± 0.08 mm/s). The latter was not expected, and was hypothesised to be due to the presence of a paramagnetic Fe^{2+} species, such as unreacted iron palmitate/iron gluconate from the iron tablets/ iron palmitate precursor. The Mössbauer spectrum of a sample of homogenised iron tablets, shown in figure 6A, did indeed show such a Fe^{2+} species, with parameters (δ = 1.20 ± 0.01 mm/s and Δ = 2.23 ± 0.01 mm/s) comparable to those observed in the product. From this analysis, we can say that although there some unreacted percursor, an appreciable amount of the precursor has formed magnetite and/or maghemite nanoparticles. The fact that these appear as a Fe^{3+} doublet rather than a magnetic sextet is most likely due to the small particle size, so that the room temperature Mössbauer measurement is above the superparamagnetic blocking temperature of the nanoparticles.

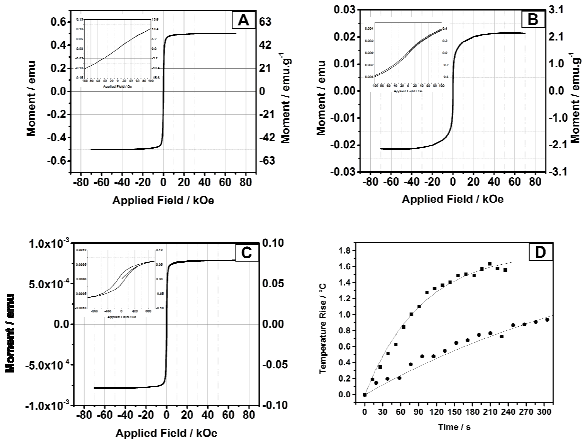

[Figure 7: SQUID magnetic hysteresis loops of: iron oxide nanoparticles from standard reagents (Sample **(I))** (A), iron oxide nanoparticles from iron palmitate decomposed in 1-octadecene (Sample **(II))** (B) and iron oxide nanoparticles obtained from the decomposition of iron palmitate in shark liver oil (Sample **(III))** (C). (D) shows magnetic hyperthermia heating of water-transferred iron oxide nanoparticles from Sample **(I)** (bottom) and nanoparticles from sample **(III)** (top). Insets are magnifications of the hysteresis loops, showing minimal coercivity.]]

Magnetic hyperthermia measurements were carried out after the nanoparticles were transferred to water. This is achieved using an amphiphilic polymer, poly(maleic anhydride-*alt*-octadecene). The hydrophobic moieties of poly(maleic anhydride-*alt*-octadecene) allow the polymer to

Faraday Discussions Accepted Manuscript

form a hydrophobic layer around individual nanoparticles through van der Waals interactions, promoted by a polar solvent, chloroform. Once wrapped around a nanoparticle, the solvent is removed, and maleic anhydride groups in the polymer backbone are opened *via* nucleophilic attack with base, rendering the nanoparticles dispersible in water.

Heat loss dissipation measurements of sample **(III)** showed a temperature rise of 1.8ºC at a prepared concentration of 2.3 mg/mL, whilst Sample **(I)** showed a temperature of 2.1ºC at a prepared concentration of 6.1 mg/mL with an Intrinsic Loss Power (ILP) values of 1.9 and 0.4 respectively, placing them towards the market leaders within the range of commercially available magnetic fluid hyperthermia agents.[37] Sample **(II)** showed signs of heat dissipation on exposure to the AC magnetic field (figure 7D). Whilst an ILP value is not as high as other values quoted in the literature, this method demonstrates a promising outlook on synthesising a low cost functional hyperthermia agent.[37]

SQUID magnetometry shows that Sample **(I)** and **(II)** are superparamagnetic at 300K. The SLO samples exhibited signs of ferromagnetic behaviour with a normalised remanance M/M_s = 0.2 and a coercivity of 100 Oe. Samples **(I)**, **(II)** and **(III)** have saturation magnetisation values of 52, 2.2 and 0.1 emu/g respectively.

Conclusions

In this article, we have successfully synthesised iron oxide nanomaterials from readily available high street sources. The synthesis occurs in two steps, namely the synthesis of the precursor, iron palmitate, and then its decomposition in the presence of surfactants and high boiling point solvents, again shop-purchased. The results from these syntheses were compared to standard techniques, and the associated costs compared (ESI Table 5). We have demonstrated that iron oxide nanomaterials can be produced at a far lower cost than standard literature techniques, at the Chemist's discretion due to the availability of the reagents used.

The nanomaterials were characterised using a variety of techniques including: XRD, XPS, EDX spectroscopy, TEM, Mössbauer spectroscopy, TGA/DSC, ATR-FTIR, SQUID, and magnetic hyperthermia measurements. High quality, monodisperse iron oxide nanocrystals were also obtained from the decomposition of iron palmitate in 1-octadecene and shark liver oil, both displaying a degree of heating on exposure to an AC magnetic field.

The inexpensive iron oxide nanomaterials obtained have tremendous scope for the transfer of this reaction to batch or mass production, for use in numerous applications from medical devices to catalysis. The good performance of the synthesised materials in magnetic hyperthermia tests give scope for the further development of cost effective iron oxide nanomaterials.

Notes and references

[a] *Materials Chemistry Research Centre, Department of Chemistry, University College London, 20 Gordon Street, London, WC1H 0AJ, UK.E-mail: I.p.parkin@ucl.ac.uk*
[b] *UCL Healthcare Biomagnetics Laboratories, Royal Institution of Great Britain, 21 Albemarle Street, London, W1S 4BS, UK*
[c] *School of Chemistry, University of East Anglia, Norwich Research Park, Norwich, NR4 7TJ, UK*.
[d] *School of Engineering and Materials Science, Queen Mary, University of London, Mile End Road, London, E1 4NS, UK*

† Electronic Supplementary Information (ESI) available: Contains additional TEM , SAED, EDX and FTIR characterisation, Differential Scanning Calorimetry curves of iron-oleate and iron-palmitate. See DOI: 10.1039/b000000x/

1. D. Ling and T. Hyeon, *Small*, 2013, **9**, 1450–1466.

2. N.-N. Song, H.-T. Yang, X. Ren, Z.-A. Li, Y. Luo, J. Shen, W. Dai, X.-Q. Zhang, and Z.-H. Cheng, *Nanoscale*, 2013, **5**, 2804–2810.

3. J. Park, K. An, Y. Hwang, J.-G. Park, H.-J. Noh, J.-Y. Kim, J.-H. Park, N.-M. Hwang, and T. Hyeon, *Nat. Mater.*, 2004, **3**, 891–895.

4. M. Mahmoudi, S. Sant, B. Wang, S. Laurent, and T. Sen, *Adv. Drug Deliv. Rev.*, January, **63**, 24–46.

5. W. Cai and J. Wan, *J. Colloid Interface Sci.*, 2007, **305**, 366–370.

6. A. Guittoum, A. Layadi, H. Tafat, and N. Souami, *J. Magn. Magn. Mater.*, 2010, **322**, 566–571.

7. A. Tavakoli, M. Sohrabi, and A. Kargari, *Chem. Pap.*, 2007, **61**, 151–170.

8. A. S. Teja and P.-Y. Koh, *Prog. Cryst. Growth Charact. Mater.*, 2009, **55**, 22–45.

9. S. Laurent, D. Forge, M. Port, A. Roch, C. Robic, L. Vander Elst, and R. N. Muller, *Chem. Rev.*, 2008, **108**, 2064–2110.

10. S. Xu, J. Ziegler, and T. Nann, *J. Mater. Chem.*, 2008, **18**, 2653–2656.

11. M. Lattuada and T. A. Hatton, *Langmuir*, 2007, **23**, 2158–2168.

12. L. M. Bronstein, X. Huang, J. Retrum, A. Schmucker, M. Pink, B. D. Stein, and B. Dragnea, *Chem. Mater.*, 2007, **19**, 3624–3632.

13. S. Sun and H. Zeng, *J. Am. Chem. Soc.*, 2002, **124**, 8204–8205.

14. J. Bear, G. Charron, M. T. Fernandez-Arguelles, S. Massadeh, P. McNaughter, and T. Nann, in *BetaSys: Systems Biology of Regulated Exocytosis in Pancreatic ß-Cells*, Springer New York, 2011, vol. 2, pp. 185–220.

15. G. Vallejo-Fernandez, O. Whear, A. G. Roca, S. Hussain, J. Timmis, V. Patel, and K. O'Grady, *J. Phys. Appl. Phys.*, 2013, **46**, 312001.

16. R. Hergt, R. Hiergeist, I. Hilger, W. A. Kaiser, Y. Lapatnikov, S. Margel, and U. Richter, *J. Magn. Magn. Mater.*, 2004, **270**, 345–357.

17. M. A. Gonzalez-Fernandez, T. E. Torres, M. Andrés-Vergés, R. Costo, P. de la Presa, C. J. Serna, M. P. Morales, C. Marquina, M. R. Ibarra, and G. F. Goya, *J. Solid State Chem.*, 2009, **182**, 2779–2784.

18. S. E. Barry, *Int. J. Hyperthermia*, 2008, **24**, 451–466.

19. L. A. Thomas, L. Dekker, M. Kallumadil, P. Southern, M. Wilson, S. P. Nair, Q. A. Pankhurst, and I. P. Parkin, *J. Mater. Chem.*, 2009, **19**, 6529.

20. I. Baker, Q. Zeng, W. Li, and C. R. Sullivan, *J. Appl. Phys.*, 2006, **99**, 08H106–08H106–3.

21.M. Gonzales-Weimuller, M. Zeisberger, and K. M. Krishnan, *J. Magn. Magn. Mater.*, 2009, **321**, 1947–1950.

22. E. E. Lees, T.-L. Nguyen, A. H. A. Clayton, B. W. Muir, and P. Mulvaney, *ACS Nano*, 2009, **3**, 2049–2049.

23. T. Pellegrino, L. Manna, S. Kudera, T. Liedl, D. Koktysh, A. L. Rogach, S. Keller, J. Rädler, G. Natile, and W. J. Parak, *Nano Lett.*, 2004, **4**, 703–707.

Faraday Discussions Accepted Manuscript

24. http://resonantcircuits.com/.

25. B. M. Wetherbee and P. D. Nichols, *Comp. Biochem. Physiol. B Biochem. Mol. Biol.*, 2000, **125**, 511–521.

26. M. J. Bakes and P. D. Nichols, *Comp. Biochem. Physiol. B Biochem. Mol. Biol.*, 1995, **110**, 267–275.

27. J. C. Cain and R. A. Morton, *Biochem. J.*, 1955, **60**, 274–283.

28. I. Batista and M. L. Nunes, *Fish. Res.*, 1992, **14**, 329–334

29. B. Rodriguez-Gonzalez, M. Spasova, M. Farle, L. Liz-Marzan, and A. Shavel, *Adv. Funct. Mater.*, 2007, **17**, 3870–3876.

30. C. Yang, J. Wu, and Y. Hou, *Chem. Commun.*, 2011, **47**, 5130–5141.

31. M. V. Kovalenko, M. I. Bodnarchuk, R. T. Lechner, G. Hesser, F. Schäffler, and W. Heiss, *J. Am. Chem. Soc.*, 2007, **129**, 6352–6353.

32. J. Cheon, N.-J. Kang, S.-M. Lee, J.-H. Lee, J.-H. Yoon, and S. J. Oh, *J Am Chem Soc*, 2004, **126**, 1950–1951.

33. L. M. Bronstein, J. E. Atkinson, A. G. Malyutin, F. Kidwai, B. D. Stein, D. G. Morgan, J. M. Perry, and J. A. Karty, *Langmuir*, 2011, **27**, 3044–3050.

34. L. J. Berchmans, M. Myndyk, K. L. Da Silva, A. Feldhoff, J. Šubrt, P. Heitjans, K. D. Becker, and V. Šepelák, *J. Alloys Compd.*, 2010, **500**, 68–73.

35. R. Dom, R. Subasri, K. Radha, and P. H. Borse, *Solid State Commun.*, 2011, **151**, 470–473.

36. Y. Sahoo, H. Pizem, T. Fried, D. Golodnitsky, L. Burstein, C. N. Sukenik, and G. Markovich, *Langmuir*, 2001, **17**, 7907–7911.

37. M. Kallumadil, M. Tada, T. Nakagawa, M. Abe, P. Southern, and Q. A. Pankhurst, *J. Magn. Magn. Mater.*, 2009, **321**, 1509–1513.

Faraday Discussions Accepted Manuscript